Earth and Space Science

RESEARCH ARTICLE
10.1029/2021EA002037

Hydromechanical Effects of Micro-Organisms on Fine-Grained Sediments During Early Burial

N. Tanner Mills[1], Julia S. Reece[1], Michael M. Tice[1], and Jason B. Sylvan[2]

[1]Department of Geology and Geophysics, Texas A&M University, College Station, TX, USA, [2]Department of Oceanography, Texas A&M University, College Station, TX, USA

Key Points:

- We experimentally determine the effects of micro-organisms on the compression and permeability behavior of fine-grained sediments
- Micro-organisms cause a small increase in compression index and small decrease in permeability for fine-grained sediments
- The degree to which micro-organisms decrease permeability in fine-grained sediments is controlled by multiple sediment properties

Correspondence to:
N. T. Mills,
tannermills@tamu.edu

Citation:
Mills, N. T., Reece, J. S., Tice, M. M., & Sylvan, J. B. (2022). Hydromechanical effects of micro-organisms on fine-grained sediments during early burial. *Earth and Space Science*, *9*, e2021EA002037. https://doi.org/10.1029/2021EA002037

Received 21 SEP 2021
Accepted 16 JAN 2022

Author Contributions:
Conceptualization: N. Tanner Mills, Julia S. Reece, Michael M. Tice, Jason B. Sylvan
Data curation: N. Tanner Mills
Formal analysis: N. Tanner Mills
Investigation: N. Tanner Mills
Methodology: N. Tanner Mills, Julia S. Reece, Michael M. Tice, Jason B. Sylvan
Project Administration: Julia S. Reece
Resources: Julia S. Reece
Supervision: Julia S. Reece, Michael M. Tice, Jason B. Sylvan
Writing – original draft: N. Tanner Mills

Abstract Micro-organisms are known to change fluid flow and permeability processes in subsurface environments, but this has only been demonstrated for coarse-grained sediments and fractures. For fine-grained sediments (mudstones), little is known about the effects of micro-organisms on hydromechanical properties. Here, we investigated the influence of micro-organisms on the porosity, permeability, and compressibility of fine-grained sediments. We performed resedimentation experiments with and without micro-organisms added to two reconstituted, fine-grained sediment samples. These sediments were collected from the Ursa and Brazos-Trinity Basins in the Gulf of Mexico during Integrated Ocean Drilling Program Expedition 308. Micro-organisms caused a systematic, yet small increase in compression index for both sediments. Changes to permeability caused by micro-organisms, while relatively minor, were greater for the Ursa sediment than the Brazos-Trinity sediment. Additionally, the effect of micro-organisms on permeability is greater at higher porosities and lower vertical effective stresses. Differences in permeability behavior between the two sediments are likely due to differences in sediment properties and nutrients for microbial growth. We therefore suggest that the effectiveness of micro-organisms at altering fluid flow in fine-grained sediments is dependent on burial depth (porosity as a function of vertical effective stress) and the grain size, pore and pore throat size, and specific surface area of a sediment. Characterizing the effects of micro-organisms on the hydromechanical properties of fine-grained sediments can further our understanding of the controls on pore pressure near the sediment–water interface in marine environments and aid in bioclogging practices around contaminated sites in terrestrial environments.

Plain Language Summary Micro-organisms dwell in the pore space between sediments (porosity) all across Earth's surface. This could potentially affect the rate at which porosity is lost as clay-rich sediments are buried (compressibility) and the ease at which fluids flow through clay-size sediments (permeability). In this paper, we investigate if and how micro-organisms change the compressibility and permeability of fine-grained sediments (sediments dominated by clay-size grains). To do this, we experimentally compress these fine-grained sediments in the vertical direction with micro-organisms added and without micro-organisms added (control experiment) while measuring sediment porosity, compressibility, and permeability. We find that micro-organisms cause a small increase in the rate of porosity loss during compression and a small decrease in permeability. However, the amount of permeability decrease caused by micro-organisms is dependent on multiple properties of the clay-size sediment. These findings can be used to help understand how water pressures in ocean sediments can become elevated, which could lead to damage of seafloor infrastructure, or benefit geotechnical engineering practices that use micro-organisms to prevent fluid flow around contaminated sediments.

1. Introduction

Micro-organisms (bacteria and archaea) are ubiquitous in marine and terrestrial sediments (e.g., Delgado-Baquerizo et al., 2018; Francis et al., 2005). In fact, active microbial cells have been found to thrive in sediments at burial depths down to a few thousand meters (Inagaki et al., 2015; Onstott et al., 1998). However, in general, the concentration of microbial cells is highest near the sediment–water interface in marine sediments or the sediment–air interface in terrestrial sediments and decreases with increasing depth (D'Hondt et al., 2004; Parkes et al., 1994; Pedersen et al., 1996). Thus, any interactions between micro-organisms and sediments are decreased at greater depths and stresses (Rebata-Landa & Santamarina, 2006).

Writing – review & editing: N. Tanner Mills, Julia S. Reece, Michael M. Tice, Jason B. Sylvan

In sediments and fractures, micro-organisms produce biofilms composed of cells and extracellular polymeric substance (Flemming & Wingender, 2010), which can affect fluid flow properties by clogging pore space (e.g., Ivanov & Chu, 2008). Biofilms have been shown to decrease permeability or hydraulic conductivity—which is directly proportional to permeability assuming constant fluid density and viscosity—by 1–3 orders of magnitude in coarse-grained sediments such as sands and silts (Brydie et al., 2005; Taylor & Jaffé, 1990; Zhong & Wu, 2013) and fractures (Cheng et al., 2021; Hill & Sleep, 2002; Ross et al., 2001). While these previous studies from the geotechnical engineering community have focused on bioclogging in sand-size sediments, the incorporation of clay-size particles into bioclogging studies has only been performed with subordinate amounts of clay-size particles (<15 wt.%) in sediments dominated by the sand-size fraction (e.g., Glatstein & Francisca, 2014; Seki et al., 1998).

The geological and geotechnical engineering communities have extensively studied the compression and permeability behaviors of fine-grained sediments, such as mudstones (Hart et al., 1995; Neuzil, 2019; Reece, 2021; Rubey & Hubbert, 1959; Skempton, 1970; Terzaghi, 1943; Yang & Aplin, 2004). Mudstones exhibit a dramatic decline in porosity within the first several hundred meters of burial followed by a gradual decline through deeper burial (Dzevanshir et al., 1986; Ingebritsen et al., 2006; Mondol et al., 2007). Additionally, the compressibility (rate of porosity loss with effective stress) of a mudstone is dependent on its grain size, grain shape, stress history, and clay mineralogy, with clay-rich mudstones being more compressible (more porosity loss) than silt-rich mudstones (Dewhurst et al., 1998; Reece, 2021). This decrease in porosity with progressive burial results in a decrease in mudstone permeability, where porosity and permeability have a log linear relationship (e.g., Neuzil, 1994, 2019; Reece et al., 2012; Schneider et al., 2011). However, the effects of micro-organisms on the compression behavior of fine-grained sediments are poorly constrained (Daniels et al., 2009) and their effects on the permeability of fine-grained sediments are unexplored.

Here, we investigate the influence of micro-organisms on the compression and permeability behavior of fine-grained sediments (mudstones). We measure porosity, permeability, and compressibility as a function of vertical effective stress for fine-grained sediments of varying compositions with and without added micro-organisms. We show that, in contrast to coarse-grained (sandy) sediments, micro-organisms do not greatly affect porosity, permeability, and compressibility in fine-grained sediments. Moreover, the relative effects of micro-organisms on sediment permeability are dependent on sediment porosity, grain size, pore and pore throat size, and specific surface area. Our results are of importance to both the geological and geotechnical engineering communities as we expand the known controls on the effectiveness of micro-organisms to affect fluid flow in marine and terrestrial environments.

2. Geologic Background

The sediment samples used in this study were collected from the Gulf of Mexico during Integrated Ocean Drilling Program (IODP) Expedition 308, which sailed in 2005. Two regions of the Gulf of Mexico were sampled and logged during this expedition (Figure 1) in order to characterize subsurface fluid flow and overpressure on the continental slope (Flemings et al., 2006). These regions include the Ursa Basin located ~230 km south-southeast of New Orleans, LA, and the Brazos-Trinity Basin IV located ~250 km south-southeast of Houston, TX (Figure 1; Flemings et al., 2006). Three sites were drilled each in the Ursa Basin (U1322, U1323, and U1324) and in the Brazos-Trinity Basin IV (U1319, U1320, and U1321; Flemings et al., 2006). This study focuses only on sediments from Sites U1324 (Hole B) and U1319 (Hole A).

At Site U1324 (Ursa Basin), two lithostratigraphic units are present. Unit I is composed of hemipelagic and turbidite levee clay and mud with intervals of mass transport deposits between 0 and 364.7 m below sea floor (mbsf; Holocene–late Pleistocene) and unit II is composed of interbedded sand and silt mass transport deposits with mud overbank deposits between 364.7 and 600.8 mbsf (late Pleistocene; Flemings et al., 2006). Cell counts of micro-organisms are highest (2×10^5 cells/cm^3_{total}; at a porosity of 0.75) near the seafloor, decrease to 1×10^4 cells/cm^3_{total} (at a porosity of 0.50) at 100 mbsf, and are below the detection limits used at the time of sampling for the remainder of the cored profile (Flemings et al., 2006). Expedition scientists suggested that these low cell counts were due to the clay-rich nature of the sediments at this site (Flemings et al., 2006).

At Site U1319 (Brazos-Trinity Basin IV), six lithostratigraphic units are present: (a) unit I, foraminifera-bearing hemipelagic clays between 0 and 3.3 mbsf (Holocene–late Pleistocene); (b) unit II, hemipelagic muds and thin

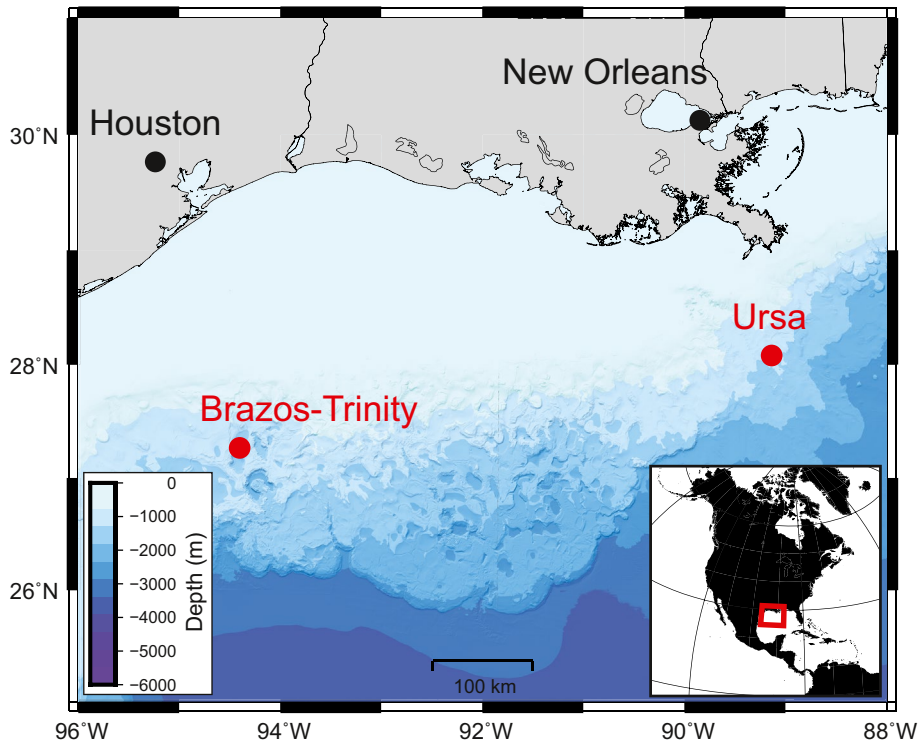

Figure 1. Bathymetry map showing the locations of Ursa and Brazos-Trinity sediments obtained from the Gulf of Mexico during Integrated Ocean Drilling Program (IODP) Expedition 308.

turbidite and mass transport deposits between 3.3 and 17.3 mbsf (late Pleistocene); (c) unit III, hemipelagic microfossil-bearing clays between 17.3 and 23.5 mbsf (late Pleistocene); (d) unit IV, hemipelagic clay and fine sand turbidite deposits between 23.5 and 29.5 mbsf (late Pleistocene); (e) unit V, hemipelagic nannofossil- and foraminifera-bearing clays between 29.5 and 31.0 mbsf (late Pleistocene); and (f) unit VI, bioturbated clays deposited by muddy plumes or nepheloid layers between 31.0 and 155.8 mbsf (late Pleistocene; Flemings et al., 2006). Cell counts of micro-organisms near the seafloor of Site U1319 are 1 order of magnitude higher (1.2×10^6 cells/cm^3_{total}; at a porosity of 0.78) than at Site U1324, but then also decrease to 1×10^4 cells/cm^3_{total} (at a porosity of 0.50) at ~100 mbsf, and are below the detection limits used at the time of sampling for the remainder of the cored profile (Flemings et al., 2006). Expedition scientists suggested that these low cell counts were due to low sedimentation rates and a lack of nutrients at this site (Flemings et al., 2006).

3. Materials and Methods

3.1. Materials

Two natural bulk mudstone powders were prepared using IODP sediments collected from the Ursa Basin (Site U1324) and the Brazos-Trinity Basin IV (Site U1319). We refer to these homogenized sediments as either the Ursa sediment or the Brazos-Trinity sediment, respectively. The Ursa sediment comes from two distinct lithostratigraphic units: (a) 1.2 kg of hemipelagic muds from lithostratigraphic unit I (subunit IA; Flemings et al., 2006) at depths of 4–32 mbsf and (b) 0.8 kg of silt and mud overbank deposits from lithostratigraphic unit II (subunit IIC; Flemings et al., 2006) at depths of 493–502 mbsf. The Brazos-Trinity sediment comes from lithostratigraphic unit II (subunits IIA, IIB, and IIC; Flemings et al., 2006) and is composed of 1.9 kg of hemipelagic muds with thin turbidite and mass transport deposits at depths of 4–13 mbsf. After collection, the samples were individually air dried, disaggregated into clay- and silt-size particles, and homogenized into these two distinct bulk mudstone powders.

3.2. Material Characterization

We characterized the dry bulk sediment powders by determining Atterberg limits, particle size distribution, and mineralogy. The Atterberg limits are known as consistency limits and are used to describe the plasticity and mechanical strength of a soil or unconsolidated mudstone. The plastic limit (*PL*) is the critical water content at which the soil or sediment changes from the semisolid to the plastic state and is determined using the hand roll method as specified in ASTM D4318-17 (ASTM International, 2017a). The liquid limit (*LL*) is the critical water content that marks the boundary between the plastic and liquid states, and it is determined using the Casagrande cup and multipoint method as specified in ASTM D4318-17 (ASTM International, 2017a). The plasticity index (*PI*) is defined as the difference between the *LL* and the *PL* and defines the range of water contents over which the unconsolidated fine-grained sediment or soil behaves plastically.

Particle size analysis is carried out using the hydrometer method as specified by ASTM D7928 (ASTM International, 2017b). This method utilizes principles from Stoke's law, namely that larger and denser particles fall out of a sediment suspension faster than smaller and less dense particles. A sediment suspension is created by mixing ~50 g of sediment, 5 g of sodium hexametaphosphate (dispersant), and nanopure water. After hydrating the sediment for 24 hr, the suspension is poured into a graduated cylinder and water is used to bring the total volume to 1,000 mL. The suspension is then vigorously mixed and timed sedimentation begins. A hydrometer is inserted into the suspension to measure specific gravity at discrete points in elapsed time. Results of hydrometer tests are given as the percent of particles in the suspension that are finer than any given particle size.

The mineralogy of the dry sediment powders is determined by X-ray diffraction (XRD). The whole rock and clay fraction (particles <2 μm) XRD analyses were performed using a Bruker D8 Advance X-ray diffractometer with a CuKα source ($\lambda = 0.154$ nm) operating at 40 kV and 40 mA. The whole rock XRD patterns were recorded from 2° to 70° 2θ with a dwell time of 3° 2θ per minute. To obtain the clay fraction, the bulk sample was first pretreated with 1 M sodium acetate at a pH of 5 in an 80°C water bath and 30% hydrogen peroxide to remove all carbonate minerals and organic matter, respectively. The clay fraction was then obtained via centrifugation after deflocculation and Na saturation with Na_2CO_3. Salts in the resultant clay fraction suspension were removed by dialysis. The clay fraction was then treated with Mg and K separately and transferred to their respective glass slides for analysis. Clay fraction XRD patterns were recorded from 2° to 32° 2θ with a dwell time of 3° 2θ per minute. These XRD spectra were recorded in the air-dried state, after the Mg saturated sample was treated with glycerol, and after the K saturated sample had been heated to 330°C and 550°C. Semiquantitative analysis was performed using the reference intensity ratio method for the bulk mineralogy and the mineral intensity factor method for the <2 μm fraction.

3.3. Resedimentation

Resedimentation experiments are used to replicate natural burial processes of fine-grained sediments (e.g., Reece, 2021; M. Santagata & Kang, 2007; Schneider et al., 2011) and follow the procedure of a traditional oedometer test as specified in ASTM Standard D2435 (ASTM International, 2020). We use this technique because it allows us to control the stress conditions acting on a mudstone, create a replicable mudstone sample (e.g., Reece, 2021; M. Santagata & Kang, 2007; M. C. Santagata et al., 2005), eliminate sample disturbance, isolate variables affecting consolidation, and perform a systematic study to address fundamental research questions.

The first step in the resedimentation process is to mix a dry mudstone powder with a pore fluid solution (explained below) to create a stable and homogeneous slurry. Water contents of 102% and 105% for the Ursa and Brazos-Trinity sediments, respectively, were identified to ensure stable slurries without gravimetric settling. The slurry is then poured into a consolidometer and incrementally, uniaxially loaded with weights to a maximum applied vertical stress of 100 kPa (10 total increments) using a load increment ratio of 1 in accordance with ASTM Standard D2435 (ASTM International, 2020; Germaine & Germaine, 2009). We loaded the slurry for 2 days each during increments 1–9 and for 4 days during increment 10 to reach end of primary consolidation. As the slurry is loaded, the pore fluids are allowed to drain through filter paper and porous stones above and below the sample. The slurry is then unloaded to an overconsolidation ratio of 4 (~25 kPa) following the increment of maximum stress. Upon completion, the sample can be extruded as a cohesive, intact mudstone. A linear displacement transducer is added during increment 4 and used to continuously measure the vertical displacement of the sample throughout compression. This transducer allows us to calculate void ratio (porosity) and compressibility

at discrete points in the experiment (load increments 4–10). The final void ratio is measured on a subsample of the extruded mudstone using the wet and dry mass technique (Blum, 1997).

We calculate intrinsic permeability at each stress level corresponding to load increments 4–10. We utilize the Log of Time theory as specified in ASTM Standard D2435 (ASTM International, 2020; Germaine & Germaine, 2009) to derive the time of 50% consolidation in a fully drained system, which is proportional to the coefficient of consolidation (c_v):

$$c_v = \frac{0.197 H_d^2}{t_{50}}, \tag{1}$$

where 0.197 is a time factor corresponding to 50% consolidation, H_d is the drainage height of the sample (half the sample height for drainage from the top and bottom of the specimen), and t_{50} is the time to 50% consolidation. Permeability (k) is then determined for each increment (increments 4–10) using c_v, the coefficient of volume compressibility (m_v; which is the change in strain over the change in vertical effective stress between two consecutive stress increments), and the viscosity of the pore fluid (μ; in calculations $\mu = 9.73 \times 10^{-4}$ Pa s):

$$k = c_v m_v \mu. \tag{2}$$

We performed resedimentation experiments with micro-organisms (biotic) and without micro-organisms (control) mixed into the slurry, and all experiments were performed in an anaerobic chamber containing 80% N_2, 15% CO_2, and 5% H_2. Before biotic or control experiments were performed, the utensils, pouring apparatus, and pieces of the resedimentation apparatus that come in contact with the slurry were sterilized either by autoclave or by wiping with 70% ethanol under UV light in a laminar flow hood. Because autoclaving the sediment could have resulted in damage to clay minerals (e.g., Lotrario et al., 1995; Trevors, 1996; Wolf et al., 1989), we did not sterilize the sediments. However, the sediments had low initial cell counts (see Section 2), were stored at the IODP core repository for over 10 years, and were stored as dry mudstone powders in our laboratory for over 1 year before they were used. This indicates that these preexisting cells were likely inactive or dead at the time of our experiments.

In the biotic experiments, we used the iron reducing bacteria *Shewanella oneidensis* MR-1 at two different cell concentrations (referred to as biotic 1x and biotic 4x) in the Ursa and Brazos-Trinity sediments. We utilized iron reducing bacteria because they are common in both terrestrial and marine environments (Lovley, 1991; Weber et al., 2006), are known to produce biofilms (Thormann et al., 2004), and were readily available in our laboratory. The *Shewanella* were cultured for 24 hr in autoclaved Lysogeny Broth medium (10 g/L tryptone, 5 g/L yeast extract, 10 g/L NaCl) and subsequently harvested via centrifugation and washed. Original cell counts were made by adjusting the cell solution to an optical density of 1.0 at a wavelength of 600 nm using a Beckman Coulter DU 730 spectrophotometer, which yields $\sim 8 \times 10^8$ cells/mL (Zeng & Tice, 2018). We admixed cells into the mudstone slurries at a concentration of $\sim 2.5 \times 10^8$ cells/cm^3_{solids} (volume of solids) for the biotic 1x experiments and at an increased concentration ($\sim$4 times the cells/cm^3_{solids}) of $\sim 1.0 \times 10^9$ cells/cm^3_{solids} for the biotic 4x experiments. The control experiments had no cells added.

The pore fluid used to make mudstone slurries was designed to be a basal medium to support *Shewanella* growth, and as a result, it had a lower ionic strength than seawater. The medium is modified from Marsili et al. (2008) and Zeng and Tice (2014) and is composed of 0.0174 g/L K_2HPO_4, 0.123 g/L $MgSO_4$ $7H_2O$, 0.227 g/L $(NH_4)_2SO_4$, 0.535 g/L NH_4Cl, 1.47 g/L $CaC1_2$ $2H_2O$, 0.5 g/L casamino acid, 3.73 mL/L Na DL-lactate (electron donor), and 5 mM $Fe(OH)_3$ (electron acceptor). The $Fe(OH)_3$ was prepared fresh by adjusting a solution of 0.17 M $FeCl_3$ to a pH of 7 with 5 M NaOH (Q. S. Fu et al., 2008). The pore fluid medium was filter sterilized, equilibrated in the anaerobic chamber, and the pH was adjusted to $\sim$7.0.

During resedimentation experiments, the effluent pore fluid was collected at the bottom of the specimen to measure pH and the concentration of Fe^{2+}. The pH was measured with a Fisherbrand accumet micro pH electrode (model 13-620-850) and the concentration of Fe^{2+} was measured using the ferrozine assay (Viollier et al., 2000). All steps for these measurements were performed immediately after collection (within <5 min) and inside the anaerobic chamber except the reading of final absorbance values for the ferrozine assay, which were collected using a BioTek ELx800 microplate reader.

3.4. Final Cell Counts

Direct cell counts were performed, following the techniques in Monteverde et al. (2018), using subsamples of the extruded mudstones after each resedimentation experiment. To do this, we took a 1 mL cell suspension—created using 8 mL of formalin and a 2 cm^3_{total} (total volume) mudstone subsample—and mixed it with 2.2 mL of 2.5% NaCl, 400 µL of detergent solution (composed of 100 mM EDTA, 100 mM sodium pyrophosphate, 1% (v/v) Tween-80), and 400 µL of methanol. This solution was shaken at 500 rpm for 10 min and then centrifuged at 3,000 *g* for 5 min to pellet the sediment. We then mixed 1,425 µL of the supernatant with 75 µL of DAPI, a DNA-binding fluorescent dye, let the mixture equilibrate for 5 min in the dark, and vacuum filtered the mixture onto 0.2 µm black polycarbonate filters. The filters were then mounted on glass slides and the cells were counted using epifluorescence light on a Zeiss Axio Imager.M2 at 1,000X magnification. The biotic 1x and biotic 4x samples were each counted until at least 200 total cells were observed (~30–40 fields of view). Alternatively, cells were counted in ~50 fields of view for the control samples, while not reaching 200 total cells, due to lower cell concentrations. Once the cells had been counted, we converted the concentrations from cells/cm^3_{total} (total volume) to cells/cm^3_{solids} (volume of solids) using the final void ratio data from each resedimentation experiment. This was required to account for differences in porosity between the beginning and end of resedimentation tests.

3.5. Microscale Imaging

After the resedimentation experiments had been completed, subsamples of the extruded mudstones were taken for scanning electron microscopy (SEM). The subsamples were taken parallel to the applied vertical stress using a standard drinking straw (minicoring technique; Lavoie et al., 1996), which were subsequently cut into 1–3 mm slices using a razor blade. These 1–3 mm slices were then immersed in 2% agarose at ~37°C and then cooled at ~4°C to solidify the agarose. We then used the resin embedding method developed by Uramoto et al. (2014) to replace the pore fluids with resin. First, this consisted of sequentially soaking the subsamples in 2.5% glutaraldehyde, 2% osmium tetroxide, and 1% uranyl acetate for 3 hr each at ~4°C with washings in between. The subsamples were then dehydrated using a series of solutions with increasing ethanol concentrations (between 30% and 100%). The ethanol was then replaced with *n*-butyl glycidyl ether (QY-1) and the QY-1 was subsequently replaced with Quetol 651 resin (details in Uramoto et al., 2014). After curing for 24 hr at 60°C, the subsamples were cut and then polished using oil-based aluminum oxide grits. The polished subsamples were coated in gold and backscatter electron (BSE) images were taken using a TESCAN VEGA 3 SEM. Images were only taken for the end-member resedimentation experiments, that is, control and biotic 4x tests.

4. Results

4.1. Material Characterization

Atterberg limits results show that *LL*, *PL*, and *PI* are 59%, 20%, and 39% for the Ursa sediment and 71%, 23%, and 48% for the Brazos-Trinity sediment, respectively (Figure 2a). Atterberg limits were performed in duplicate, with water content errors for both samples being <0.5%, and their results are presented as averages. Both sediment samples are classified as high plasticity clays (Figure 2a). Hydrometer tests for the Ursa sediment yielded an average of 59% of particles finer than 2 µm (by mass), while the Brazos-Trinity sediment yielded an average of 65% of particles finer than 2 µm (by mass; Figure 2b). The hydrometer tests were also performed in duplicate, with the error of the percent of particles finer than 2 µm for both samples being <1.5%. Because two hydrometer tests cannot be easily averaged, we display both hydrometer tests for each sediment sample in Figure 2b. The bulk mineralogy of both the Ursa and Brazos-Trinity sediments is dominated by quartz and clay minerals, with subordinate amounts of feldspar, calcite, and dolomite (Figures 2c and 2d). In the <2 µm fraction, the Ursa sediment contains more illite than smectite and the Brazos-Trinity sediment contains more smectite than illite (Figures 2c and 2d). The hydrometer and mineralogy data for the Ursa sediment were previously published in Mills et al. (2021), where this sediment was referred to as the Gulf of Mexico sediment.

4.2. Compression and Permeability Behavior

Compression curves for the Ursa and Brazos-Trinity sediments with bacteria (biotic 1x and biotic 4x) and without bacteria (control) display similar trends: void ratio (e; $e = n/(1 - n)$, where n is porosity) linearly decreases with

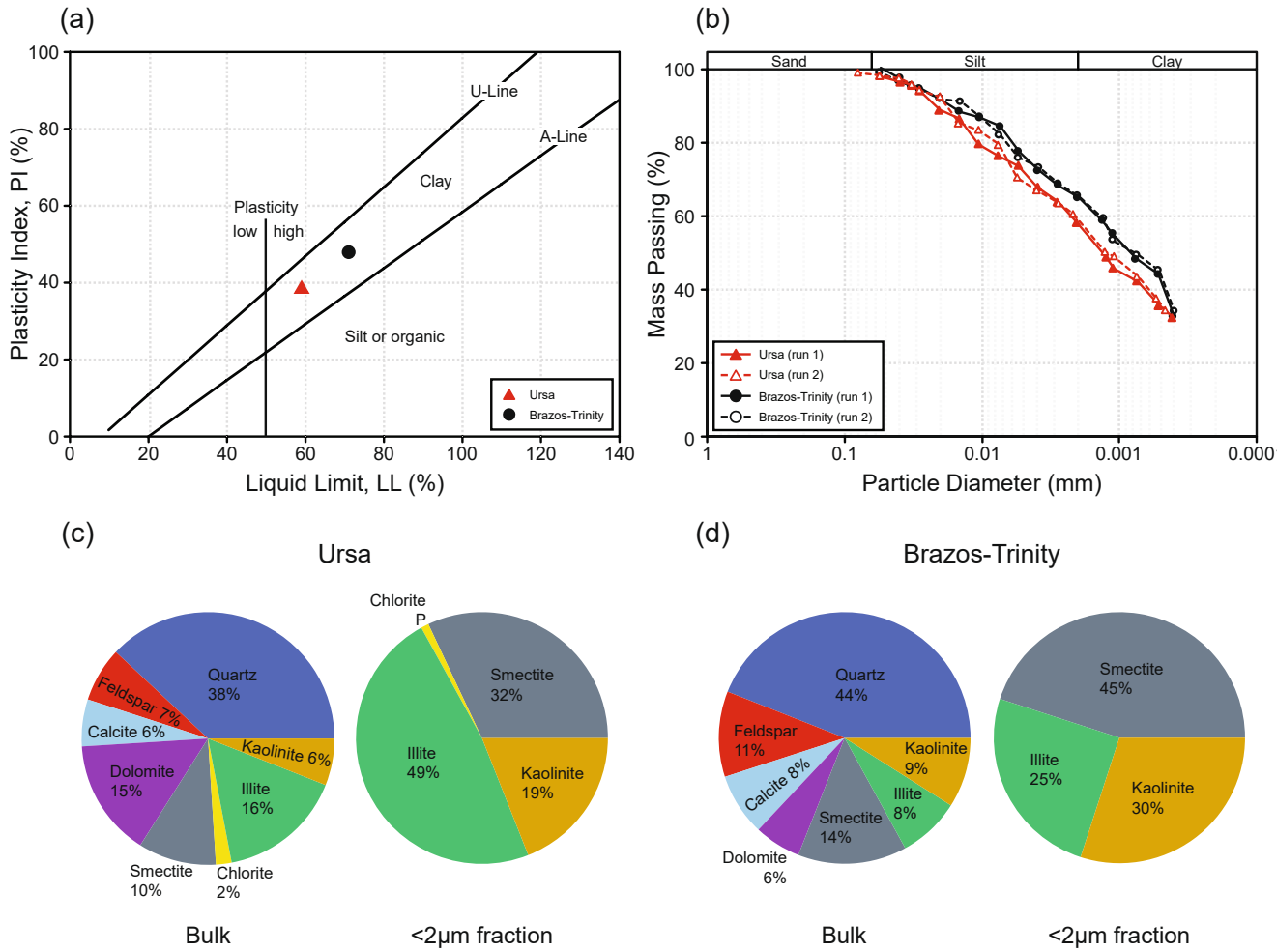

Figure 2. Material characterization results for the Ursa and Brazos-Trinity sediments. (a) Plasticity chart showing Atterberg limits results. The U-line marks the upper limit of correlation between plasticity index and liquid limit and the A-line marks the boundary between clayey (above) and silty or organic (below) sediments. (b) Particle size distributions from hydrometer tests. Both hydrometer tests for each sediment sample are shown because two tests for the same sample cannot easily be averaged without interpolation due to measurements at different particle size diameters. (c) Bulk and clay-size fraction (<2 μm) mineralogy for the Ursa mudstone powder. (d) Bulk and clay-size fraction (<2 μm) mineralogy for the Brazos-Trinity mudstone powder. P, present but not quantified.

increasing logarithm of vertical effective stress (σ_v'; Figure 3a). This compression trend follows the commonly observed behavior in sediments during burial (Burland, 1990; Skempton, 1970; Terzaghi, 1943), which can be modeled with the equation:

$$e = e_0 - C_c \log_{10}\left(\frac{\sigma_v'}{\sigma_0'}\right), \tag{3}$$

where e_0 and σ_0' are empirically derived parameters and the compression index (C_c) is the slope of the compression line. Here, we define σ_0' at 1 kPa and constrain C_c over a vertical effective stress range of 2.5–100 kPa. While both of these sediments display similar compression trends, they show distinct ranges of e and C_c values (Figure 3a). The initial void ratios measured at σ_v' of 2.5 kPa (e_i) for the Ursa sediment range between 2.15 and 2.23 and void ratios decrease with added stress down to 1.17–1.21 at σ_v' of 100 kPa (Figure 3a and Table 1). For the Brazos-Trinity sediment, e_i values range between 2.36 and 2.48 and void ratios decrease with added stress down to 1.34–1.35 at σ_v' of 100 kPa (Figure 3a and Table 1). Compression indices, determined by fitting the $e - \log(\sigma_v')$ model (Equation 3) to the data, range between 0.60 and 0.66 and between 0.64 and 0.72 for Ursa and Brazos-Trinity sediments, respectively (Figure 3b and Table 1). The lower C_c values for the Ursa sediment indicate that this sediment is stiffer than the Brazos-Trinity sediment. In contrast, the expansion indices (C_e; slope between e and

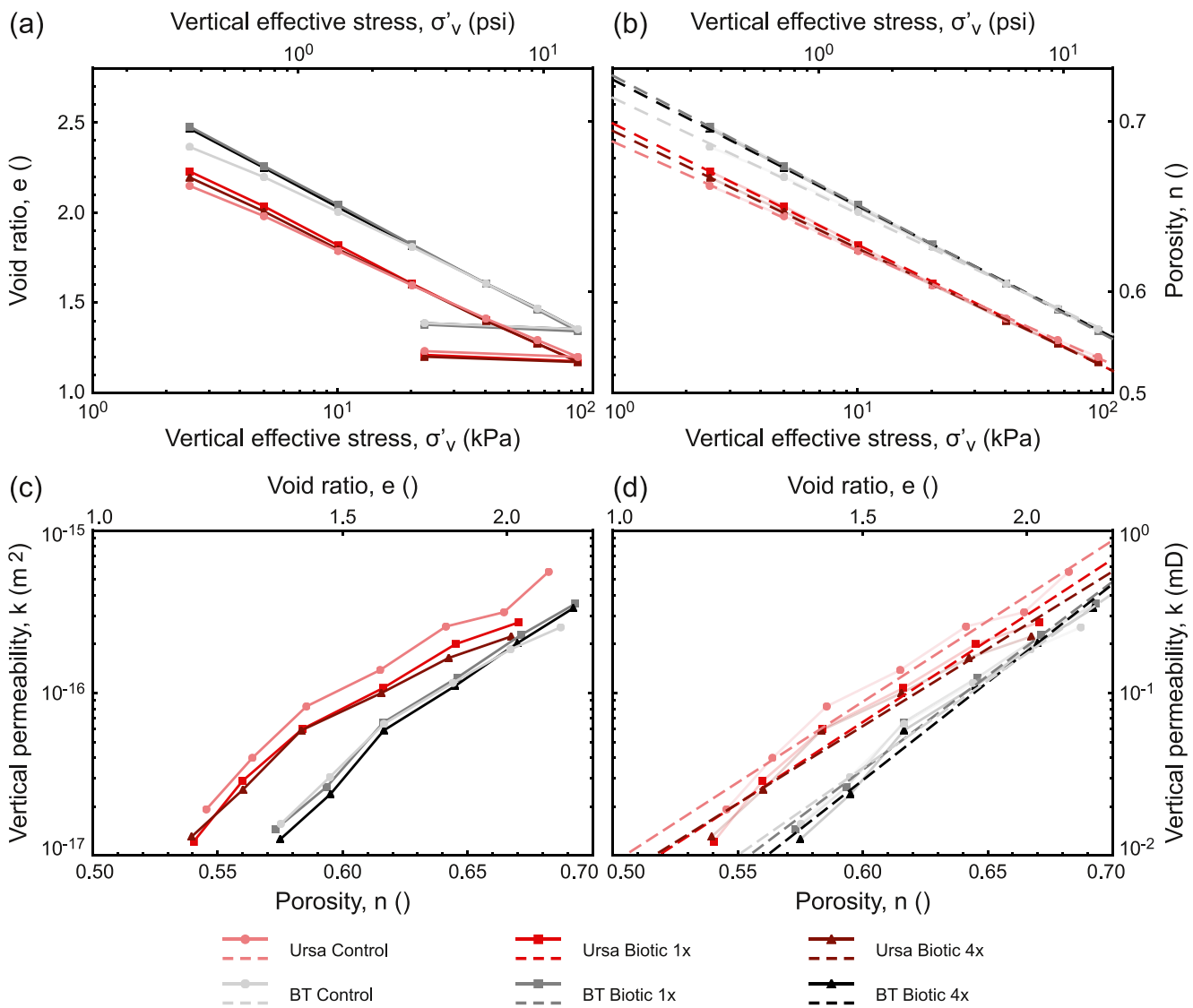

Figure 3. (a, b) Compression and (c, d) permeability–porosity behavior of the Ursa and Brazos-Trinity sediments for control, biotic 1x, and biotic 4x circumstances. Measured compression and permeability–porosity data (markers and solid lines) are displayed in (a) and (c), respectively. The best fit lines (dashed lines) from the compression and permeability–porosity models (Equations 3 and 4) are displayed in (b) and (d), respectively. Modeled compression (e_0 and C_c) and permeability–porosity (γ and k_0) fitting parameters are presented in Table 1 for each resedimentation test. The measured data were obtained during resedimentation increments 4–10. BT, Brazos-Trinity.

$\log(\sigma_v')$ during the unloading phase of the resedimentation experiments) for both sediments fall within a similar range (~0.05–0.06; Figure 3a and Table 1).

The addition of bacteria slightly changes the compression behavior of the Ursa and Brazos-Trinity sediments. For both sediments, e_i is increased and e at 100 kPa is decreased with the addition of bacteria. These changes result in increasing C_c values with additions of bacteria during resedimentation tests (Figure 3b and Table 1). Specifically, for both sediments, C_c increases by ~0.06 from the control resedimentation test to both biotic resedimentation tests, which had similar C_c values (Figure 3b and Table 1). The varying e_i and C_c values result in a crossover of compression curves for the Ursa and Brazos-Trinity sediments at σ_v' values of ~30 and ~40 kPa, respectively (Figures 3a and 3b). The C_e values for both sediments show no trends between the control, biotic 1x, and biotic 4x experiments (Figure 3a and Table 1).

The permeability–porosity behavior of the Ursa and Brazos-Trinity sediments with and without bacteria display similar trends: the permeability decreases logarithmically as porosity decreases (Figure 3c). This permeability–

Table 1
Compression and Permeability Results From the Ursa and Brazos-Trinity Resedimentation Experiments for Control, Biotic 1x, and Biotic 4x Circumstances

		Compression					Permeability		
Sample	Test	e_0	e_i	C_c	R^2 (for C_c)	C_e	γ	R^2 (for γ)	Log(k_0) (m^2)
Ursa	Control	2.39	2.15	0.60	0.999	0.051	9.94	0.975	−22.02
	Biotic 1x	2.50	2.23	0.66	0.999	0.057	10.05	0.965	−22.21
	Biotic 4x	2.45	2.20	0.65	0.999	0.047	9.54	0.965	−21.93
Brazos-Trinity	Control	2.64	2.36	0.64	0.999	0.053	10.76	0.979	−22.92
	Biotic 1x	2.76	2.48	0.72	1.000	0.059	11.06	0.987	−23.44
	Biotic 4x	2.74	2.47	0.70	0.999	0.054	12.09	0.986	−23.79

Note. e_0, void ratio at a vertical effective stress of 1 kPa; e_i, first measured void ratio at a vertical effective stress of 2.5 kPa, C_c, compression index (constrained over vertical effective stresses of 2.5 and 100 kPa); C_e, expansion index (constrained over vertical effective stresses of 25 and 100 kPa); γ, fitted slope of the (log)permeability–porosity relationship; log(k_0), the fitted intercept of the (log)permeability–porosity relationship at a porosity of 0; R^2, coefficient of determination.

porosity relationship is commonly observed in mudstones during burial (e.g., Neuzil, 1994, 2019; Reece et al., 2012; Schneider et al., 2011), and it can be modeled with the equation:

$$\log_{10}(k) = \gamma\, n + \log_{10}(k_0), \tag{4}$$

where γ is the slope and k_0 is the permeability at a porosity of 0. Both sediments display distinct ranges in permeability for a given porosity (Figure 3c and Table 1). Measured permeabilities of the Ursa sediment range between 5.6×10^{-16} and 1.2×10^{-17} m^2 for a respective porosity range of 0.68–0.54, while measured permeabilities of the Brazos-Trinity sediment range between 3.5×10^{-16} and 1.3×10^{-17} m^2 for a respective porosity range of 0.69–0.57 (Figure 3c). The γ values, determined by fitting the log linear permeability–porosity model (Equation 4) to the data, range between 9.54–10.05 and 10.76–12.09 for the Ursa and Brazos-Trinity sediments, respectively (Figure 3d and Table 1). Similarly, log(k_0) values for the Ursa and Brazos-Trinity sediments range between 21.93 and 22.21 and between 22.92 and 23.79, respectively (Table 1).

The addition of bacteria influenced the permeability values at a given porosity for the Ursa sediment, while the addition of bacteria had little to no influence on the permeability of the Brazos-Trinity sediment (Figure 3c). For the Ursa sediment, the measured permeabilities at high porosities (~0.65) in the biotic 1x and biotic 4x tests are 1.3 and 1.5 times lower than that of the control test, respectively (Figure 3c). This difference is reduced at lower porosities (~0.55) where the permeabilities of both the biotic 1x and biotic 4x tests are 1.2 times lower than that of the control test (Figure 3c). For the Brazos-Trinity sediment, the measured permeability values are similar for the control, biotic 1x, and biotic 4x tests at high porosities (Figure 3c). In fact, the control sample has a lower permeability than the biotic 1x and biotic 4x samples between porosities of 0.65 and 0.69 (Figure 3c). However, below a porosity of 0.65, the biotic 4x sample has a lower permeability than that of the biotic 1x sample, which has only slightly lower or similar permeabilities as the control sample (Figure 3c). At a porosity of ~0.59, the permeability of the biotic 4x sample is 1.2 times lower than that of the biotic 1x and control samples, similar to the Ursa data at lower porosities (Figure 3c). The fitting parameters γ and k_0 show no trends for the Ursa resedimentation tests (Figure 3d and Table 1). For the Brazos-Trinity tests, γ increases and the logarithmic value of k_0 decreases from control to biotic 1x to biotic 4x (Figure 3d and Table 1).

4.3. Scanning Electron Microscopy

The microstructure of the Ursa and Brazos-Trinity sediments under control and biotic 4x conditions (lowest and highest concentrations of added bacterial cells) was investigated using BSE images. In general, both sediments display similar microstructures between their respective control and biotic 4x images (Figure 4). Three types of grains can be identified in all samples, including framework grains (quartz, calcite, or feldspar; 4–10 μm in diameter), larger elongate grains (micas or clay minerals; high aspect ratios; 10–30 μm in length), and a

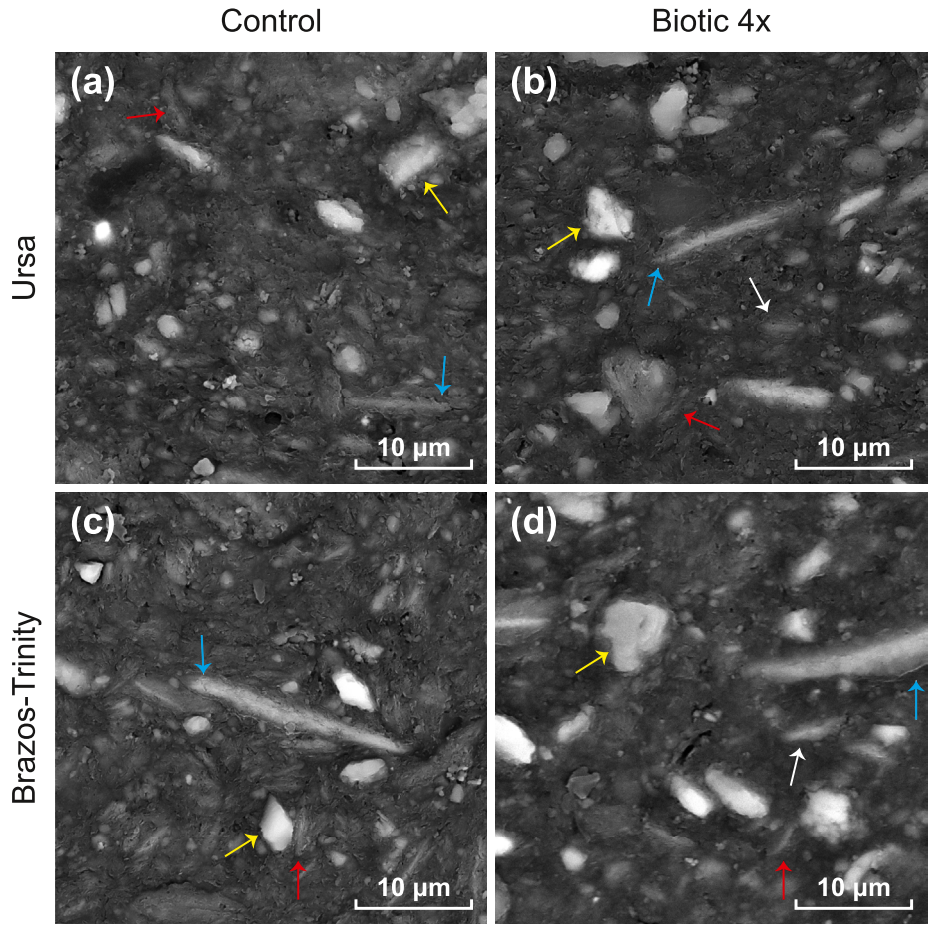

Figure 4. Backscatter electron (BSE)-scanning electron microscopy (SEM) images showing the microstructure of the extruded resedimentation samples after loading to a vertical effective stress of ~100 kPa. (a) Ursa control sample, (b) Ursa biotic 4x sample, (c) Brazos-Trinity control sample, and (d) Brazos-Trinity biotic 4x sample. The images are oriented with the applied load going from top to bottom. Yellow arrows point to framework grains, blue arrows point to elongate grains oriented perpendicular to the applied load, red arrows point to elongate grains in the clay matrix that align around framework grains, and white arrows point to diffuse grain boundaries.

clay mineral matrix (<2 μm in length; Figure 4). The framework grains (yellow arrows in Figure 4) are evenly dispersed throughout both sediments confirming that no settling occurred during resedimentation. In both sediments, larger elongate grains are nearly oriented perpendicular to the direction of the applied vertical stress (blue arrows in Figure 4), while smaller particles in the clay matrix are oriented in this fashion only far from framework grains (Figure 4). However, near framework grains, smaller particles in the clay matrix align around the framework grains (red arrows in Figure 4).

The clay matrix in the biotic 4x images for both sediments appears darker (i.e., less electron charging) and the grain boundaries within the clay matrix appear more diffuse (white arrows in Figures 4b and 4d) than in the control samples. The pore space is difficult to distinguish from the clay matrix for both sediments, especially in the biotic 4x images. This is due to the resin used to solidify the samples. However, our resin embedding method (see Section 3.5) was necessary to preserve the microstructure of our samples without desiccation and cracking. Despite these limitations, pore sizes appear to be <1 μm in diameter in the clay matrix and between 1 and 4 μm in diameter adjacent to the larger framework grains. We do not observe any bacteria, biofilms, or precipitates under these sample preparation and imaging conditions.

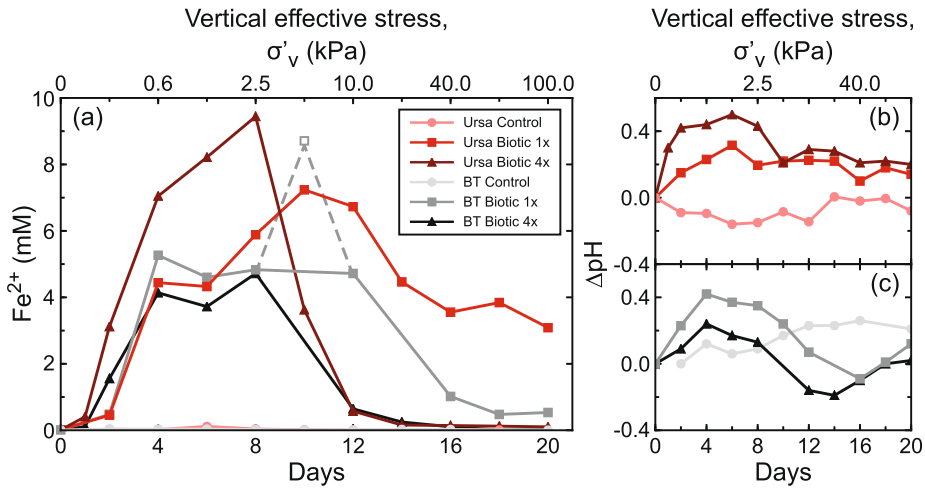

Figure 5. Pore fluid geochemistry results for the Ursa and Brazos-Trinity sediments under control, biotic 1x, and biotic 4x circumstances. (a) The concentration of Fe^{2+} throughout each resedimentation experiment. (b) The ΔpH (change in pH from beginning of each experiment) values for the Ursa control, biotic 1x, and biotic 4x tests. (c) The ΔpH values for the Brazos-Trinity control, biotic 1x, and biotic 4x tests. The open marker indicates a potentially false data point in the Brazos-Trinity biotic 1x test and the dashed lines show the potential trends to and from that data point. These data were obtained during resedimentation increments 1–10. BT, Brazos-Trinity.

4.4. Pore Fluid Geochemistry and Geomicrobiology

The concentration of Fe^{2+} in the pore fluid effluent is used to monitor bacterial activity and chemical conditions in our resedimentation experiments. As the bacteria used in our biotic resedimentation experiments reduce Fe^{3+} in the form of $Fe(OH)_3$ and oxidize lactate ($CH_3CHOHCOO^-$), Fe^{2+} is produced (e.g., Lovley et al., 1989):

$$4Fe(OH)_3 + CH_3CHOHCOO^- + 7H^+ \rightarrow 4Fe^{2+} + HCO_3^- + CH_3COO^- + 10H_2O. \quad (5)$$

For the Ursa and Brazos-Trinity sediments, the Fe^{2+} concentrations in the control tests remain low (<0.1 mM) throughout the experiments (Figure 5a). In contrast, the Fe^{2+} concentrations in the biotic tests for both sediments initially rise over the first 8–10 days, followed by a subsequent decline over the remainder of the experiments (Figure 5a). The biotic 1x and biotic 4x tests from the Ursa sediment reach maximum Fe^{2+} concentrations of 7 and 9 mM, respectively, while the biotic 1x and biotic 4x tests from the Brazos-Trinity sediment reach lower maximum Fe^{2+} concentrations of 5 mM for both (Figure 5a). Interestingly, the Fe^{2+} concentrations in the biotic 4x tests for both sediments reach their maximum values and subsequently decline to lower values in a shorter period of time than the Fe^{2+} concentrations in the biotic 1x tests for both sediments (Figure 5a).

We also monitored bacterial activity and chemical conditions by measuring the change in the effluent pH (ΔpH) from the beginning of each resedimentation experiment. As the bacteria in our biotic resedimentation experiments drive Fe reduction, they increase pore fluid pH via the consumption of H^+ (Equation 5). For the Ursa sediment, ΔpH in the control test remains constant throughout the experiment (between 0 and −0.15; Figure 5b). In the biotic 1x and biotic 4x tests, ΔpH increases over the first 6 days to respective maximum values of 0.32 and 0.50, slightly drops from days 6 through 10, and then remains constant for the remainder of the experiments (Figure 5b). For the Brazos-Trinity sediment, ΔpH in the control test gradually increases throughout the experiment from 0 to 0.25 (Figure 5c). In the biotic 1x and biotic 4x tests, ΔpH initially increases over the first 4 days to respective maximum values of 0.37 and 0.24, declines from days 4 to 15 to respective minimum values of −0.1 and −0.2, and then gradually increases for the remainder of the experiments (Figure 5c).

The final cell counts from the extruded mudstones, along with initial concentrations of cells inoculated into each resedimentation experiment, are shown in Table 2. The final cell counts for the Ursa and Brazos-Trinity sediments yielded over an order of magnitude more cells/cm^3_{solids} in the biotic 1x tests than the control tests and the biotic 4x tests yielded slightly more cells/cm^3_{solids} than the biotic 1x tests (Table 2).

Table 2
The Initial Concentrations of Bacterial Cells Inoculated Into Each Resedimented Sample and the Results for the Final Cell Counts at the End of Each Experiment

Sample	Test	Inoculation concentration (cells/cm^3_{solids})	Final cell count (cells/cm^3_{solids})
Ursa	Control	0	2.29×10^6
	Biotic 1x	2.45×10^8	2.73×10^7
	Biotic 4x	9.80×10^8	3.87×10^7
Brazos-Trinity	Control	0	2.17×10^6
	Biotic 1x	2.52×10^8	3.05×10^7
	Biotic 4x	1.01×10^9	4.34×10^7

Note. Cell concentrations are given in cells per volume of solids (cm^3). The volume of solids is the volume composed of solid particles only. This is to account for porosity differences and allow for direct comparisons between the beginning and end of a resedimentation experiment.

5. Discussion

5.1. Bacterial Growth

Based on our pore fluid geochemistry and geomicrobiology measurements, we show that the bacteria used in our experiments respired Fe^{3+} and likely produced biofilms (e.g., Thormann et al., 2004). In the biotic experiments, Fe^{2+} concentrations increased as a result of microbial iron reduction (Figure 5 and Equation 5). In fact, the bacteria reduced all 5 mM of the seeded $Fe(OH)_3$ in both sediments and an additional 2–4 mM in the Ursa sediment, likely due to preexisting Fe^{3+} in the Ursa sediment (Figure 5). The addition of 4 times the bacterial cells from the biotic 1x to biotic 4x experiments for both sediments resulted in a quicker rise and subsequent fall of Fe^{2+} concentrations (Figure 5a). The darker appearance of the clay matrix in the biotic 4x BSE images could perhaps be due to the microbial reduction of $Fe(OH)_3$ causing less electron scattering than in the control images (Figure 4). Microbial iron reduction also resulted in an increase in pH that was coincident with increasing Fe^{2+} concentrations (Figure 5).

The final cell counts for the control experiments (Table 2) are similar to the cell counts obtained from IODP data reports for the Ursa (6×10^5 cells/cm^3_{solids}; converted from cells/cm^3_{total} at a porosity of 0.75) and Brazos-Trinity (4.3×10^6 cells/cm^3_{solids}; converted from cells/cm^3_{total} at a porosity of 0.78) sites at the depths our sediments were obtained from (see Section 2). It is likely that these natural cells were largely inactive or dead at the time of our resedimentation experiments, as evidenced by unchanging pH values and Fe^{2+} concentrations in our control experiments (Figure 5), due to our sediment preparation and storage techniques (see Section 3.1). Not only were the added cells in our biotic experiments active (Figure 5), but the final cell counts for each biotic experiment (biotic 1x and biotic 4x) were over an order of magnitude higher than those of the control experiments for both sediments (Table 2). These geochemical and geomicrobiological data indicate that changes to sediment compression and permeability behavior were due to the addition of bacteria, given that all other parameters were kept constant and only the concentration of bacterial cells was changed between each experiment.

5.2. Compression Behavior

Micro-organisms cause small, yet systematic changes in compression behavior. The addition of micro-organisms results in an increase in C_c but relatively constant C_e for both sediment types (Table 1 and Figure 3), indicating that micro-organisms affect the elasto-plastic behavior of sediments, but not their elastic behavior. Perhaps the increase in C_c is due to micro-organisms increasing porosity at lower vertical effective stresses, while at higher effective stresses microbial activity could be limited by the increasing load (e.g., Rebata-Landa & Santamarina, 2006). The observation that sediments become more compressible (or less stiff) with added micro-organisms is consistent with some results from Daniels et al. (2009), who showed that C_c values increase with increasing amounts of biofilm for a lean clay (with sand-size grains present) but not for a sand–bentonite mixture (65% sand; 35% bentonite). While their results are inconclusive, our results clarify and affirm that micro-organisms increase C_c.

5.3. Permeability

Several processes could explain the fact that the addition of micro-organisms caused greater absolute changes to permeability at a given porosity for the Ursa sediment than for the Brazos-Trinity sediment (Figures 3c and 3d). For example, sedimentological and physical property differences between the two sediments could be responsible for this observed behavior. The Brazos-Trinity sediment has a smaller average grain size than the Ursa sediment (65% vs. 59% of particles <2 μm; Figure 2) and, as a result, has smaller pores and pore throats (Dewhurst et al., 1999) and a larger specific surface area (Mayer & Rossi, 1982). In fact, specific surface area (S_a) calculated for the Ursa and Brazos-Trinity sediments from their *LL* values after Santamarina et al. (2002) yielded respective S_a values of 72.2 and 93.8 m^2/g. These S_a values reflect the differences in the <2 μm fraction between the two sediments, which is dominated by illite for the Ursa sediment and by smectite for the Brazos-Trinity sediment.

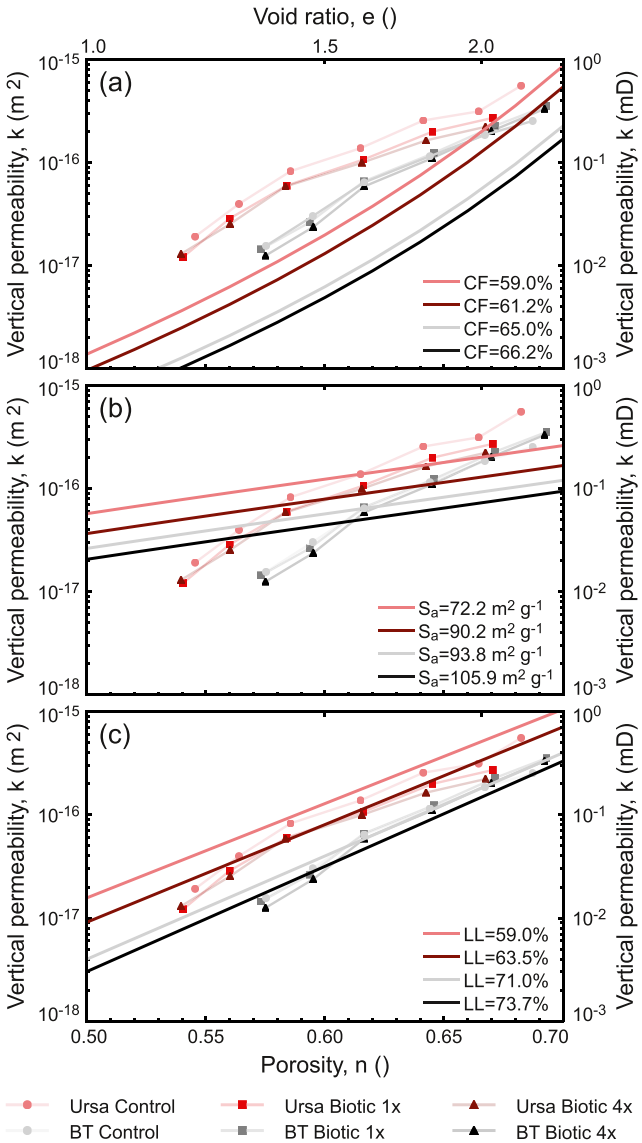

Figure 6. Permeability models from literature show that small changes in (a) clay fraction (*CF*; % of grains <2 μm; Yang & Aplin, 2010), (b) specific surface area (S_a; Kozeny–Carman equation; assumed tortuosity factors of 0.11 and 0.15 for the Ursa and Brazos-Trinity sediments, respectively; Daigle & Dugan, 2009), and (c) liquid limit (*LL*; Casey et al., 2013) are needed to match the greatest difference in permeability caused by micro-organisms in the Ursa (at porosity of 0.65) and Brazos-Trinity (at porosity of 0.58) sediments (model equations shown in Table 3). The measured permeability–porosity data from our experiments are displayed with semitransparent lines behind the modeled permeability–porosity curves displayed with solid lines. The salmon and light gray colored solid curves indicate the modeled permeability–porosity relationships using measured *CF*, S_a, and *LL* data (see Sections 4.1 and 5.3 for data; Table 3) from the Ursa and Brazos-Trinity sediments (approximates the control experiments), respectively. The maroon and black colored solid curves indicate the modeled permeability–porosity relationships at increased values (to match permeability change due to micro-organisms) of *CF*, S_a, and *LL* for the Ursa and Brazos-Trinity sediments, respectively.

Therefore, it is likely that these smaller pores and pore throats make it harder for micro-organisms to survive under increasing vertical stress (Ivanov & Chu, 2008; Park & Santamarina, 2020; Phadnis & Santamarina, 2011) and that as sediment S_a goes up the produced biofilm covers more of the increased particle surface area and protrudes less into the open pore space. This would indicate that biofilms are less effective at decreasing permeability in sediments with smaller pores and pore throats and larger S_a.

Another explanation for the larger impact of micro-organisms on the permeability of the Ursa sediment than the Brazos-Trinity sediment could be a difference in the amount of bioavailable nutrients or the spatial distribution of those nutrients. More Fe^{3+} was reduced in the biotic samples from the Ursa sediment than the Brazos-Trinity sediment (see Section 5.1 and Figure 5), despite both sediments having the same amount of synthesized Fe^{3+} added to them (5 mM of $Fe(OH)_3$). The excess of naturally occurring bioavailable Fe^{3+} or its spatial distribution in the Ursa sediment could have caused biofilms to have a greater effect on permeability, especially at higher porosities, compared to the biotic samples from the Brazos-Trinity sediments which had less naturally occurring bioavailable Fe^{3+} (Figure 5). This inferred increase in biofilm growth or the differences in the spatial distribution of biofilms, combined with differences in sediment properties, are likely the reasons that micro-organisms had a greater effect on permeability in the Ursa sediment. Strikingly, changes in sediment properties resulted in larger permeability differences between the Ursa and Brazos-Trinity sediments than the addition of micro-organisms to an individual sediment (Figures 3c and 3d).

The effect of micro-organisms on permeability varies with porosity. For the Ursa sediment, permeability is more impacted by micro-organisms at higher porosities than at lower porosities, which can be observed by the convergence of regression lines toward lower porosities (Figures 3c and 3d). Several processes could explain this behavior. First, lower porosities at increased vertical stress could restrict habitable pore space for micro-organisms and potentially puncture them (e.g., Rebata-Landa & Santamarina, 2006). Second, it could be due to the exhaustion of $Fe(OH)_3$ as evidenced by a decrease in Fe^{2+} concentrations over the second half of the Ursa biotic experiments (Figure 5). A lack of nutrients such as $Fe(OH)_3$ (for Fe-reducing micro-organisms) can cause deterioration of biofilms and can result in a relative increase in permeability (Castegnier et al., 2006). Finally, it could be due to decreasing cell concentrations from the beginning to the end of our biotic experiments (Table 2), which is likely a result of decreased nutrients. In the Brazos-Trinity sediment, the Fe^{2+} and cell concentrations also decrease during the later stages of the biotic experiments (Figure 5 and Table 2). However, in this sample, micro-organisms appear to have a minimal effect on permeability at all porosities (Figures 3c and 3d), which is in contrast to the Ursa sediment and is likely due to the decreased grain and pore size as discussed above.

We further place permeability changes in our sediments caused by micro-organisms into context using permeability models from literature that depend on sediment properties, including clay fraction (*CF*; % of grains <2 μm by mass; Yang & Aplin, 2010), S_a (Daigle & Dugan, 2009), and *LL* (Casey et al., 2013; Figure 6; model equations shown in Table 3). We measured original *CF* and *LL* values for both of our sediments prior to our experiments using hydrometer and Atterberg limits techniques (see Sections 3.2 and 4.1), respectively. Original S_a values were calculated for each sediment sample using their respective *LL* values and an empirical relationship between S_a

Table 3
The Permeability Models, Their References, and the Original and Increased Clay Fraction (CF), Specific Surface Area (S_a), and Liquid Limit (LL) Values Used in Figure 6

Model	Reference	Values used		
		Variable	Ursa	Brazos-Trinity
$Ln(k) = -69.59 - 26.79CF + 44.07CF^{0.5} + (-53.61 - 80.03CF + 132.78CF^{0.5})\ e + (86.61 + 81.91CF - 163.61CF^{0.5})e^{0.5}$	Yang and Aplin (2010)	*CF* original	59.0%	65.0%
		CF increased	61.2%	66.2%
$k = \frac{n^3}{\nu\tau^2\rho_g^2(1-n)^2S_a^2}$	Daigle and Dugan (2009)	S_a original	72.2 $m^2\ g^{-1}$	93.8 $m^2\ g^{-1}$
		S_a increased	90.2 $m^2\ g^{-1}$	105.9 $m^2\ g^{-1}$
$Log_{10}(k) = (0.072LL + 4.9)\ (n - 0.5) - 7.4\ log_{10}(LL) - 3.7$	Casey et al. (2013)	*LL* original	59.0%	71.0%
		LL increased	63.5%	73.7%

Note. k, permeability; n, porosity; e, void ratio; *CF*, clay fraction; S_a, specific surface area; *LL*, liquid limit. S_a was calculated using the equation: $S_a = 1.8LL - 34$ (Santamarina et al., 2002). For the Daigle and Dugan (2009) model, variables are defined as follows: ν, dimensionless pore shape factor; τ, tortuosity; ρ_g, grain density. $\nu\tau^2$ was assumed to be 0.11 and 0.15 for the Ursa and Brazos-Trinity sediments, respectively.

and *LL* proposed by Santamarina et al. (2002). We then determined the changes in these sediment properties needed to match the greatest change in permeability created by micro-organisms for each sediment (change from their respective *CF*, S_a, and *LL* values; Table 3). Specifically, the largest permeability differences in the Ursa and Brazos-Trinity sediments occur at porosities of 0.64 and 0.58, respectively. At these porosities, the permeabilities of the biotic 4x samples are 1.5 and 1.2 times lower than those of the control samples. In order to account for these same permeability differences in the Ursa and Brazos-Trinity sediments, *CF* would need to be increased by 2.2% and 1.2% (Figure 6a and Table 3; Yang & Aplin, 2010), S_a would need to be increased by 24.9% and 12.9% (Figure 6b and Table 3; Daigle & Dugan, 2009), and *LL* would need to be increased by 4.5% and 2.7% (Figure 6c and Table 3; Casey et al., 2013), respectively. These models illustrate that the influence of micro-organisms on sediment permeability is relatively small for our two fine-grained sediment samples and equates to small changes in *CF*, S_a, and *LL* (Figure 6 and Table 3). Ultimately, the effects of micro-organisms on sediment permeability are likely lessened for increasingly finer-grained sediments, for example, from the Ursa sediment to Brazos-Trinity sediment.

Incidentally, the *LL* model from Casey et al. (2013) fits our measured control data for both sediments better than the *CF* (Yang & Aplin, 2010) and S_a (Daigle & Dugan, 2009) models. This is not surprising as *LL* reflects both the quantity and type of clay minerals present in a mudstone (Casey et al., 2013) and, therefore, combines the effects of clay-size fraction and S_a, which is a function of mineralogy, into a single model parameter.

5.4. Conceptual Model

We propose a new conceptual model for biofilm distributions at the pore scale that integrates previous work on sandstones/siltstones and fractures with our new observations for fine-grained sediments (mudstones; Figure 7). Previous experimental work using sandstones/siltstones or fractures have demonstrated a large decrease in permeability with the addition of micro-organisms (e.g., Brydie et al., 2005; Cheng et al., 2021; Hill & Sleep, 2002; Taylor & Jaffé, 1990). In contrast, our experimental work using mudstones has demonstrated a small decrease in permeability with the addition of micro-organisms (Figure 3). Despite these differences, microbial cell concentrations are similar across all studies. For instance, experiments using sandstones/siltstones or fractures have utilized cell concentrations ranging from 1.5×10^5 to 1×10^9 cells/mL (Brydie et al., 2005; Ross et al., 2001; Zhong & Wu, 2013). Initial cell concentrations for our experiments using mudstones (Table 2) fit within the higher end of that range with cell concentrations $>9 \times 10^7$ cells/$cm^3_{\text{pore fluid}}$ (converted from cells/cm^3_{solids} for direct comparison; Table 2). Therefore, the differences in permeability reduction caused by micro-organisms between our experiments using mudstones and previous experiments using sandstones/siltstones or fractures are likely controlled by factors other than microbial cell concentrations, such as the distributions of biofilm, which is dependent on physical and textural properties of the sediments.

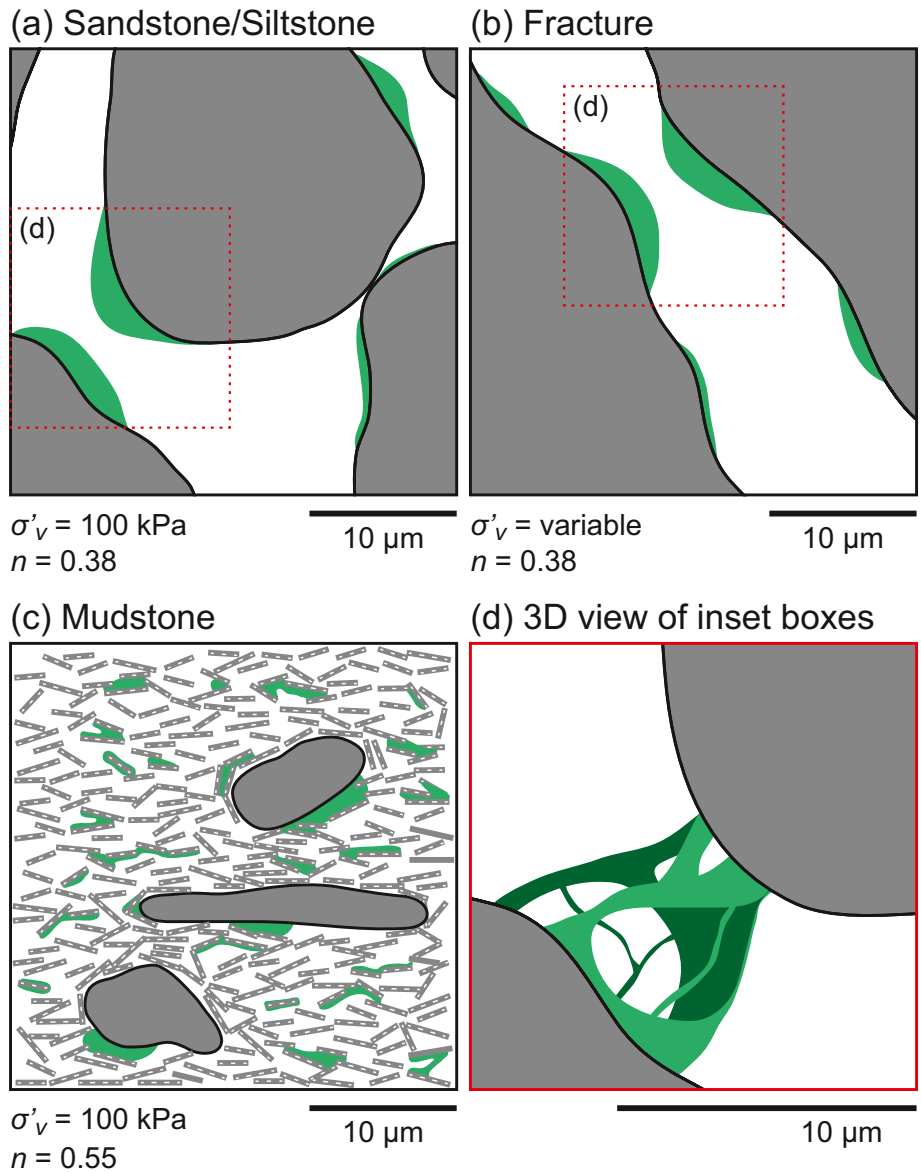

Figure 7. A conceptual model showing the two-dimensional pore-scale effects of biofilm on a (a) sandstone or siltstone, (b) fracture, and (c) mudstone. (d) Zoomed-in view from the inset boxes in (a) and (b) that is more indicative of three-dimensional (3D) biofilm distribution in natural pores. Biofilms are green and sediments are gray. Each of the illustrations in (a)–(c) contains the same area of biofilm. The (a) sandstone/siltstone and (c) mudstone illustrations contain respective porosities of 0.38 and 0.55, which are both indicative of burial to a vertical effective stress of 100 kPa (Ingebritsen et al., 2006; Mondol et al., 2007). The (a) sandstone/siltstone and (b) fracture illustrations have the same porosity. Vertical effective stress (σ'_v) and porosity (n) for the illustrations in (a)–(c) are located below each of the respective illustrations. The theoretical fluid flow is from the bottom to the top of each illustration.

In our conceptual model, the sandstone/siltstone and fracture have large grains, large pores and pore throats, low S_a, and few flow paths (Figures 7a and 7b). As a result, biofilm covers the available surface area and grows out into the large pores and pore throats and occludes porosity (Figures 7a and 7b), which causes a significant decrease in permeability. It should be noted that in our sandstone/siltstone and fracture illustrations, the biofilms occluding pore space are simplified (Figures 7a and 7b), while they are more complex in three-dimensional pores in nature (Figure 7d; e.g., Hand et al., 2008; Harrison et al., 2011).

In contrast, the mudstone illustration has grains of various shapes and sizes, small pores and pore throats, high S_a, and multiple flow paths (Figure 7c), which are all evidenced in our BSE images (Figure 4). In this scenario,

we hypothesize that biofilm is spread out over a large surface area and fills only a small portion of the available pore space (Figure 7c). Despite a larger tortuosity, the high number of flow paths in the mudstone indicates that pores filled with biofilm could potentially even be bypassed (Figure 7c). For these reasons, micro-organisms have a lessened effect on mudstone permeability than they do on coarser-grained sediments and fractures. Therefore, grain size, specific surface area, pore and pore throat size, and the number of flow paths—all of which could potentially be moderated by (clay) mineralogy—are likely to control changes in permeability due to micro-organisms.

5.5. Implications

We have shown that micro-organisms have a larger effect on the permeability of fine-grained sediments at lower stresses, that is, higher porosities (Figure 3). For fine-grained sediments near the sediment–water interface in marine or lacustrine settings, these porosities could be even higher (0.75–0.80; Boggs, 2009) than measured in our experiments, leading to an even greater reduction in permeability due to the presence of micro-organisms. This effect could be amplified in sediments with higher concentrations of nutrients and microbial cells (e.g., Haglund et al., 2003; Kallmeyer et al., 2012; Montagna, 1982) than used in our experiments. The decrease in permeability caused by micro-organisms near the sediment–water interface could prevent fluxes of aqueous chemical species (e.g., carbon, nitrogen, sulfur, iron, and phosphorous) between the sediments and the overlying water column. Moreover, a decrease in permeability and an increase in compression index, which was also observed in our data (Figure 3), are both independent parameters known to increase pore pressure within sediments during consolidation (Broichhausen et al., 2005). Overpressured pore fluids in the shallow subsurface could cause sediment gravity flows or even submarine landslides (Dugan & Flemings, 2000; Flemings et al., 2008), which in turn have the potential to damage seafloor infrastructure. However, at lower porosities in fine-grained sediments, this effect on pore pressure would be diminished.

Our results also have significance for terrestrial environments and geotechnical engineering practices. At porosities more indicative of fine-grained terrestrial soils (<0.55; e.g., Foti & Lancellotta, 2004; Y. Fu et al., 2019), it is likely that micro-organisms have a lessened effect on permeability. Further, adding micro-organisms to fine-grained terrestrial soils, as has been hypothesized for coarser-grained soils or fracture systems to prevent fluid flow around radioactive waste sites (Coombs et al., 2008; Harrison et al., 2011) and contaminated areas (Kanmani et al., 2014; Ross & Bickerton, 2002) or on precarious slopes (Ivanov & Chu, 2008), may not be as useful and effective in reducing permeability compared to coarser-grained soils and fractures. Given that micro-organisms have been shown to decrease fluid flow in coarser-grained sediments and fractures and that our results show that micro-organisms have a limited effect on permeability in finer-grained sediments at lower porosities (<0.55), there is likely a grain size threshold at which micro-organisms no longer have a significant impact on permeability.

6. Conclusions

We used resedimentation experiments to document the effects of micro-organisms on the compression and permeability behavior of fine-grained sediments. Key findings include the following:

1. The pore fluid geochemistry and geomicrobiology data indicate that micro-organisms respired and likely developed biofilms in the biotic experiments of both sediments.
2. The addition of micro-organisms resulted in small, yet systematic changes in compression behavior, as evidenced by an increase in C_c of ~0.06 for both of our sediments.
3. The addition of micro-organisms resulted in a greater absolute permeability reduction in the Ursa sediment than in the Brazos-Trinity sediment, which is likely due to differences in sediment properties and the amount of microbial activity between the two sediments.
4. The effect of micro-organisms on permeability is greater at higher porosities and lower vertical effective stresses.
5. The effectiveness of micro-organisms in decreasing permeability is not as great in fine-grained sediments compared to coarse-grained sediments and is controlled by sediment grain size, pore and pore throat size, specific surface area, and porosity.

Data Availability Statement

Our experimental resedimentation and pore fluid geochemistry data are available in the Zenodo repository (https://doi.org/10.5281/zenodo.5519839).

Acknowledgments
This research used samples provided by the International Ocean Discovery Program (IODP). Funding for this research was provided to J. Reece by the American Chemical Society Petroleum Research Fund (#55617-DNI8) and in part by the National Science Foundation Division of Ocean Sciences (#1945011) as well as to N. T. Mills by a Michel T. Halbouty research grant from the American Association of Petroleum Geologists Grants-in-Aid Program. We thank Dr Youjun Deng and Bidemi Fashina for their help with X-ray diffraction analyses in the Department of Soil and Crop Sciences at Texas A&M University and Dr Stanislav Vitha for his help with scanning electron microscopy work at the Microscopy and Imaging Center at Texas A&M University. We also thank Lucky Marchelino, Jesse Yeon, Tate Ryan, Gunner Boler, Andrew Robertson, and Charles Holmes for their help in the laboratory.

References

ASTM International. (2017a). Standard test methods for liquid limit, plastic limit, and plasticity index of soils (D4318). In *Annual book of ASTM standards. Soil and rock (I)* (p. 20). West Conshohocken, PA: American Society for Testing and Materials. https://doi.org/10.1520/D4318-17E01

ASTM International. (2017b). Standard test methods for particle-size distribution (gradation) of fine-grained soils using the sedimentation (hydrometer) analysis (D7928). In *Annual book of ASTM standards. Soil and rock (I)* (p. 25). West Conshohocken, PA: American Society for Testing and Materials. https://doi.org/10.1520/D7928-17

ASTM International. (2020). Standard test methods for one-dimensional consolidation properties of soils using incremental loading (D2435/D2435M). In *Annual book of ASTM standards. Soil and rock (I)* (p. 14). West Conshohocken, PA: American Society for Testing and Materials. https://doi.org/10.1520/D2435-20

Blum, P. (1997). Physical properties handbook: A guide to the shipboard measurement of physical properties of deep-sea cores. *Ocean Drilling Program Technical Note*, *26*. https://doi.org/10.2973/odp.tn.26.1997

Boggs, S. (2009). *Petrology of sedimentary rocks* (2nd ed., p. 600). Cambridge University Press. https://doi.org/10.1017/CBO9780511626487

Broichhausen, H., Littke, R., & Hantschel, T. (2005). Mudstone compaction and its influence on overpressure generation, elucidated by a 3D case study in the North Sea. *International Journal of Earth Sciences*, *94*(5), 956–978. https://doi.org/10.1007/s00531-005-0014-1

Brydie, J. R., Wogelius, R. A., Merrifield, C. M., Boult, S., Gilbert, P., Allison, D., & Vaughan, D. J. (2005). The µ2M project on quantifying the effects of biofilm growth on hydraulic properties of natural porous media and on sorption equilibria: An overview. *Geological Society of London, Special Publications*, *249*(1), 131–144. https://doi.org/10.1144/GSL.SP.2005.249.01.11

Burland, J. B. (1990). On the compressibility and shear strength of natural clays. *Géotechnique*, *40*(3), 329–378. https://doi.org/10.1680/geot.1990.40.3.329

Casey, B., Germaine, J. T., Flemings, P. B., Reece, J. S., Gao, B., & Betts, W. (2013). Liquid limit as a predictor of mudrock permeability. *Marine and Petroleum Geology*, *44*, 256–263. https://doi.org/10.1016/j.marpetgeo.2013.04.008

Castegnier, F., Ross, N., Chapuis, R. P., Deschênes, L., & Samson, R. (2006). Long-term persistence of a nutrient-starved biofilm in a limestone fracture. *Water Research*, *40*(5), 925–934. https://doi.org/10.1016/j.watres.2005.12.038

Cheng, Y., Chou, C., Voltolini, M., Borglin, S., Ajo-Franklin, J. B., & Wu, Y. (2021). Flow and permeability evolution during microbial sulfate reduction and inhibition in fractured rocks. *Energy & Fuels*, *35*(3), 1989–1997. https://doi.org/10.1021/acs.energyfuels.0c01787

Coombs, P., West, J. M., Wagner, D., Turner, G., Noy, D. J., Milodowski, A. E., et al. (2008). Influence of biofilms on transport of fluids in subsurface granitic environments—Some mineralogical and petrographical observations of materials from column experiments. *Mineralogical Magazine*, *72*(1), 393–397. https://doi.org/10.1180/minmag.2008.072.1.393

Daigle, H., & Dugan, B. (2009). Extending NMR data for permeability estimation in fine-grained sediments. *Marine and Petroleum Geology*, *26*(8), 1419–1427. https://doi.org/10.1016/j.marpetgeo.2009.02.008

Daniels, J. L., Cherukuri, R., & Ogunro, V. O. (2009). Consolidation and strength characteristics of biofilm amended barrier soils. In E. K. Yanful (Ed.), *Appropriate technologies for environmental protection in the developing world: Selected papers from ERTEP 2007, July 17–19 2007, Ghana, Africa* (pp. 257–270). Dordrecht, The Netherlands: Springer. https://doi.org/10.1007/978-1-4020-9139-1_25

Delgado-Baquerizo, M., Oliverio, A. M., Brewer, T. E., Benavent-González, A., Eldridge, D. J., Bardgett, R. D., et al. (2018). A global atlas of the dominant bacteria found in soil. *Science*, *359*(6373), 320. https://doi.org/10.1126/science.aap9516

Dewhurst, D. N., Aplin, A. C., & Sarda, J.-P. (1999). Influence of clay fraction on pore-scale properties and hydraulic conductivity of experimentally compacted mudstones. *Journal of Geophysical Research*, *104*(B12), 29261–29274. https://doi.org/10.1029/1999JB900276

Dewhurst, D. N., Aplin, A. C., Sarda, J.-P., & Yang, Y. (1998). Compaction-driven evolution of porosity and permeability in natural mudstones: An experimental study. *Journal of Geophysical Research*, *103*(B1), 651–661. https://doi.org/10.1029/97JB02540

D'Hondt, S., Jørgensen, B. B., Miller, D. J., Batzke, A., Blake, R., Cragg, B. A., et al. (2004). Distributions of microbial activities in deep subseafloor sediments. *Science*, *306*(5705), 2216–2221. https://doi.org/10.1126/science.1101155

Dugan, B., & Flemings, P. B. (2000). Overpressure and fluid flow in the New Jersey continental slope: Implications for slope failure and cold seeps. *Science*, *289*(5477), 288–291. https://doi.org/10.1126/science.289.5477.288

Dzevanshir, R. D., Buryakovskiy, L. A., & Chilingarian, G. V. (1986). Simple quantitative evaluation of porosity of argillaceous sediments at various depths of burial. *Sedimentary Geology*, *46*(3), 169–175. https://doi.org/10.1016/0037-0738(86)90057-6

Flemings, P. B., Behrmann, J. H., John, C. M., & Scientists, E. (2006). *Proceedings of the Integrated Ocean Drilling Program 308*. College Station, TX: Integrated Ocean Drilling Program Management International, Inc.

Flemings, P. B., Long, H., Dugan, B., Germaine, J., John, C. M., Behrmann, J. H., & IODP Expedition 308 Scientists. (2008). Pore pressure penetrometers document high overpressure near the seafloor where multiple submarine landslides have occurred on the continental slope, offshore Louisiana, Gulf of Mexico. *Earth and Planetary Science Letters*, *269*(3), 309–325. https://doi.org/10.1016/j.epsl.2007.12.005

Flemming, H.-C., & Wingender, J. (2010). The biofilm matrix. *Nature Reviews Microbiology*, *8*(9), 623–633. https://doi.org/10.1038/nrmicro2415

Foti, S., & Lancellotta, R. (2004). Soil porosity from seismic velocities. *Géotechnique*, *54*(8), 551–554. https://doi.org/10.1680/geot.2004.54.8.551

Francis, C. A., Roberts, K. J., Beman, J. M., Santoro, A. E., & Oakley, B. B. (2005). Ubiquity and diversity of ammonia-oxidizing archaea in water columns and sediments of the ocean. *Proceedings of the National Academy of Sciences of the United States of America*, *102*(41), 14683–14688. https://doi.org/10.1073/pnas.0506625102

Fu, Q. S., Boonchayaanant, B., Tang, W., Trost, B. M., & Criddle, C. S. (2008). Simple menaquinones reduce carbon tetrachloride and iron (III). *Biodegradation*, *20*(1), 109–116. https://doi.org/10.1007/s10532-008-9204-4

Fu, Y., Tian, Z., Amoozegar, A., & Heitman, J. (2019). Measuring dynamic changes of soil porosity during compaction. *Soil and Tillage Research*, *193*, 114–121. https://doi.org/10.1016/j.still.2019.05.016

Germaine, J. T., & Germaine, A. V. (2009). *Geotechnical laboratory measurements for engineers* (p. 351). Hoboken, NJ: John Wiley & Sons. https://doi.org/10.1002/9780470548790

Glatstein, D. A., & Francisca, F. M. (2014). Hydraulic conductivity of compacted soils controlled by microbial activity. *Environmental Technology*, *35*(15), 1886–1892. https://doi.org/10.1080/09593330.2014.885583

Haglund, A.-L., Lantz, P., Törnblom, E., & Tranvik, L. (2003). Depth distribution of active bacteria and bacterial activity in lake sediment. *FEMS Microbiology Ecology*, *46*(1), 31–38. https://doi.org/10.1016/S0168-6496(03)00190-9

Hand, V. L., Lloyd, J. R., Vaughan, D. J., Wilkins, M. J., & Boult, S. (2008). Experimental studies of the influence of grain size, oxygen availability and organic carbon availability on bioclogging in porous media. *Environmental Science & Technology*, *42*(5), 1485–1491. https://doi.org/10.1021/es072022s

Harrison, H., Wagner, D., Yoshikawa, H., West, J. M., Milodowski, A. E., Sasaki, Y., et al. (2011). Microbiological influences on fracture surfaces of intact mudstone and the implications for geological disposal of radioactive waste. *Mineralogical Magazine*, *75*(4), 2449–2466. https://doi.org/10.1180/minmag.2011.075.4.2449

Hart, B. S., Flemings, P. B., & Deshpande, A. (1995). Porosity and pressure: Role of compaction disequilibrium in the development of geopressures in a Gulf Coast Pleistocene basin. *Geology*, *23*(1), 45–48. https://doi.org/10.1130/0091-7613(1995)023<0045:PAPROC>2.3.CO;2

Hill, D. D., & Sleep, B. E. (2002). Effects of biofilm growth on flow and transport through a glass parallel plate fracture. *Journal of Contaminant Hydrology*, *56*(3), 227–246. https://doi.org/10.1016/S0169-7722(01)00210-8

Inagaki, F., Hinrichs, K. U., Kubo, Y., Bowles, M. W., Heuer, V. B., Hong, W. L., et al. (2015). Exploring deep microbial life in coal-bearing sediment down to ~2.5 km below the ocean floor. *Science*, *349*(6246), 420–424. https://doi.org/10.1126/science.aaa6882

Ingebritsen, S. E., Sanford, W. E., & Neuzil, C. E. (2006). *Groundwater in geologic processes* (2nd ed., p. 536). Cambridge, UK: Cambridge University Press.

Ivanov, V., & Chu, J. (2008). Applications of microorganisms to geotechnical engineering for bioclogging and biocementation of soil in situ. *Reviews in Environmental Science and Bio/Technology*, *7*(2), 139–153. https://doi.org/10.1007/s11157-007-9126-3

Kallmeyer, J., Pockalny, R., Adhikari, R. R., Smith, D. C., & D'Hondt, S. (2012). Global distribution of microbial abundance and biomass in subseafloor sediment. *Proceedings of the National Academy of Sciences of the United States of America*, *109*(40), 16213–16216. https://doi.org/10.1073/pnas.1203849109

Kanmani, S., Gandhimathi, R., & Muthukkumaran, K. (2014). Bioclogging in porous media: Influence in reduction of hydraulic conductivity and organic contaminants during synthetic leachate permeation. *Journal of Environmental Health Science and Engineering*, *12*(1), 126. https://doi.org/10.1186/s40201-014-0126-2

Lavoie, D. M., Baerwald, R. J., Hulbert, M. H., & Bennett, R. H. (1996). A drinking-straw mini-corer for sediments. *Journal of Sedimentary Research*, *66*(5), 1030. https://doi.org/10.2110/jsr.66.1030

Lotrario, J. B., Stuart, B. J., Lam, T., Arands, R. R., O'Connor, O. A., & Kosson, D. S. (1995). Effects of sterilization methods on the physical characteristics of soil: Implications for sorption isotherm analyses. *Bulletin of Environmental Contamination and Toxicology*, *54*, 668–675. https://doi.org/10.1007/BF00206097

Lovley, D. R. (1991). Dissimilatory Fe(III) and Mn(IV) reduction. *Microbiological Reviews*, *55*(2), 259–287. https://doi.org/10.1128/mr.55.2.259-287.1991

Lovley, D. R., Phillips, E. J. P., & Lonergan, D. J. (1989). Hydrogen and formate oxidation coupled to dissimilatory reduction of iron or manganese by *Alteromonas putrefaciens*. *Applied and Environmental Microbiology*, *55*(3), 700–706. https://doi.org/10.1128/aem.55.3.700-706.1989

Marsili, E., Baron, D. B., Shikhare, I. D., Coursolle, D., Gralnick, J. A., & Bond, D. R. (2008). *Shewanella* secretes flavins that mediate extracellular electron transfer. *Proceedings of the National Academy of Sciences of the United States of America*, *105*(10), 3968–3973. https://doi.org/10.1073/pnas.0710525105

Mayer, L. M., & Rossi, P. M. (1982). Specific surface areas in coastal sediments: Relationships with other textural factors. *Marine Geology*, *45*(3), 241–252. https://doi.org/10.1016/0025-3227(82)90112-8

Mills, N. T., Reece, J. S., & Tice, M. M. (2021). Clay minerals modulate early carbonate diagenesis. *Geology*, *49*(8), 1015–1019. https://doi.org/10.1130/G48713.1

Mondol, N. H., Bjørlykke, K., Jahren, J., & Høeg, K. (2007). Experimental mechanical compaction of clay mineral aggregates—Changes in physical properties of mudstones during burial. *Marine and Petroleum Geology*, *24*(5), 289–311. https://doi.org/10.1016/j.marpetgeo.2007.03.006

Montagna, P. A. (1982). Sampling design and enumeration statistics for bacteria extracted from marine sediments. *Applied and Environmental Microbiology*, *43*(6), 1366–1372. https://doi.org/10.1128/aem.43.6.1366-1372.1982

Monteverde, D. R., Sylvan, J. B., Suffridge, C., Baronas, J. J., Fichot, E., Fuhrman, J., et al. (2018). Distribution of extracellular flavins in a coastal marine basin and their relationship to redox gradients and microbial community members. *Environmental Science & Technology*, *52*(21), 12265–12274. https://doi.org/10.1021/acs.est.8b02822

Neuzil, C. E. (1994). How permeable are clays and shales? *Water Resources Research*, *30*(2), 145–150. https://doi.org/10.1029/93WR02930

Neuzil, C. E. (2019). Permeability of clays and shales. *Annual Review of Earth and Planetary Sciences*, *47*(1), 247–273. https://doi.org/10.1146/annurev-earth-053018-060437

Onstott, T. C., Phelps, T. J., Colwell, F. S., Ringelberg, D., White, D. C., Boone, D. R., et al. (1998). Observations pertaining to the origin and ecology of microorganisms recovered from the deep subsurface of Taylorsville Basin, Virginia. *Geomicrobiology Journal*, *15*(4), 353–385. https://doi.org/10.1080/01490459809378088

Park, J., & Santamarina, J. C. (2020). The critical role of pore size on depth-dependent microbial cell counts in sediments. *Scientific Reports*, *10*(1), 21692. https://doi.org/10.1038/s41598-020-78714-3

Parkes, R. J., Cragg, B. A., Bale, S. J., Getlifff, J. M., Goodman, K., Rochelle, P. A., et al. (1994). Deep bacterial biosphere in Pacific Ocean sediments. *Nature*, *371*(6496), 410–413. https://doi.org/10.1038/371410a0

Pedersen, K., Arlinger, J., Ekendahl, S., & Hallbeck, L. (1996). 16S rRNA gene diversity of attached and unattached bacteria in boreholes along the access tunnel to the Äspö hard rock laboratory, Sweden. *FEMS Microbiology Ecology*, *19*(4), 249–262. https://doi.org/10.1111/j.1574-6941.1996.tb00217.x

Phadnis, H. S., & Santamarina, J. C. (2011). Bacteria in sediments: Pore size effects. *Géotechnique Letters*, *1*(4), 91–93. https://doi.org/10.1680/geolett.11.00008

Rebata-Landa, V., & Santamarina, J. C. (2006). Mechanical limits to microbial activity in deep sediments. *Geochemistry, Geophysics, Geosystems*, *7*, Q11006. https://doi.org/10.1029/2006GC001355

Reece, J. S. (2021). The impact of grain size on the hydromechanical behavior of mudstones. *Geochemistry, Geophysics, Geosystems*, *22*(8), e2021GC009732. https://doi.org/10.1029/2021GC009732

Reece, J. S., Flemings, P. B., Dugan, B., Long, H., & Germaine, J. T. (2012). Permeability–porosity relationships of shallow mudstones in the Ursa Basin, northern deepwater Gulf of Mexico. *Journal of Geophysical Research*, *117*, B12102. https://doi.org/10.1029/2012JB009438

Ross, N., & Bickerton, G. (2002). Application of biobarriers for groundwater containment at fractured bedrock sites. *Remediation Journal*, *12*(3), 5–21. https://doi.org/10.1002/rem.10031

Ross, N., Villemur, R., Deschênes, L., & Samson, R. (2001). Clogging of a limestone fracture by stimulating groundwater microbes. *Water Research*, *35*(8), 2029–2037. https://doi.org/10.1016/S0043-1354(00)00476-0

Rubey, W. W., & Hubbert, M. K. (1959). Role of fluid pressure in mechanics of overthrust faulting, Part 2. Overthrust belt in geosynclinal are of western Wyoming in light of fluid-pressure hypothesis. *The Geological Society of America Bulletin*, *70*(2), 167–205. https://doi.org/10.1130/0016-7606(1959)70[167:ROFPIM]2.0.CO;2

Santagata, M., & Kang, Y. I. (2007). Effects of geologic time on the initial stiffness of clays. *Engineering Geology*, *89*(1), 98–111. https://doi.org/10.1016/j.enggeo.2006.09.018

Santagata, M. C., Germaine, J. T., & Ladd, C. C. (2005). Factors affecting the initial stiffness of cohesive soils. *Journal of Geotechnical and Geoenvironmental Engineering*, *131*(4), 430–441. https://doi.org/10.1061/(ASCE)1090-0241(2005)131:4(430)

Santamarina, J. C., Klein, K. A., Wang, Y. H., & Prencke, E. (2002). Specific surface: Determination and relevance. *Canadian Geotechnical Journal*, *39*(1), 233–241. https://doi.org/10.1139/t01-077

Schneider, J., Flemings, P. B., Day-Stirrat, R. J., & Germaine, J. T. (2011). Insights into pore-scale controls on mudstone permeability through resedimentation experiments. *Geology*, *39*(11), 1011–1014. https://doi.org/10.1130/G32475.1

Seki, K., Miyazaki, T., & Nakano, M. (1998). Effects of microorganisms on hydraulic conductivity decrease in infiltration. *European Journal of Soil Science*, *49*(2), 231–236. https://doi.org/10.1046/j.1365-2389.1998.00152.x

Skempton, A. W. (1970). The consolidation of clays by gravitational compaction. *Quarterly Journal of the Geological Society of London*, *125*(1–4), 373–411. https://doi.org/10.1144/gsjgs.125.1.0373

Taylor, S. W., & Jaffé, P. R. (1990). Biofilm growth and the related changes in the physical properties of a porous medium: 1. Experimental investigation. *Water Resources Research*, *26*(9), 2153–2159. https://doi.org/10.1029/WR026i009p02153

Terzaghi, K. (1943). Theory of consolidation. In *Theoretical soil mechanics* (pp. 265–296). John Wiley & Sons, Inc.

Thormann, K. M., Saville, R. M., Shukla, S., Pelletier, D. A., & Spormann, A. M. (2004). Initial phases of biofilm formation in *Shewanella oneidensis* MR-1. *Journal of Bacteriology*, *186*(23), 8096–8104. https://doi.org/10.1128/JB.186.23.8096-8104.2004

Trevors, J. T. (1996). Sterilization and inhibition of microbial activity in soil. *Journal of Microbiological Methods*, *26*, 53–59. https://doi.org/10.1016/0167-7012(96)00843-3

Uramoto, G.-I., Morono, Y., Uematsu, K., & Inagaki, F. (2014). An improved sample preparation method for imaging microstructures of fine-grained marine sediment using microfocus X-ray computed tomography and scanning electron microscopy. *Limnology and Oceanography: Methods*, *12*(7), 469–483. https://doi.org/10.4319/lom.2014.12.469

Viollier, E., Inglett, P. W., Hunter, K., Roychoudhury, A. N., & Van Cappellen, P. (2000). The ferrozine method revisited: Fe(II)/Fe(III) determination in natural waters. *Applied Geochemistry*, *15*(6), 785–790. https://doi.org/10.1016/S0883-2927(99)00097-9

Weber, K. A., Achenbach, L. A., & Coates, J. D. (2006). Microorganisms pumping iron: Anaerobic microbial iron oxidation and reduction. *Nature Reviews Microbiology*, *4*, 752–764. https://doi.org/10.1038/nrmicro1490

Wolf, D. C., Dao, T. H., Scott, H. D., & Lavy, T. L. (1989). Influence of sterilization methods on selected soil microbiological, physical, and chemical properties. *Journal of Environmental Quality*, *18*, 39–44. https://doi.org/10.2134/jeq1989.00472425001800010007x

Yang, Y., & Aplin, A. C. (2004). Definition and practical application of mudstone porosity–effective stress relationships. *Petroleum Geoscience*, *10*(2), 153–162. https://doi.org/10.1144/1354-079302-567

Yang, Y., & Aplin, A. C. (2010). A permeability–porosity relationship for mudstones. *Marine and Petroleum Geology*, *27*(8), 1692–1697. https://doi.org/10.1016/j.marpetgeo.2009.07.001

Zeng, Z., & Tice, M. M. (2014). Promotion and nucleation of carbonate precipitation during microbial iron reduction. *Geobiology*, *12*(4), 362–371. https://doi.org/10.1111/gbi.12090

Zeng, Z., & Tice, M. M. (2018). Electron transfer strategies regulate carbonate mineral and micropore formation. *Astrobiology*, *18*(1), 28–36. https://doi.org/10.1089/ast.2016.1560

Zhong, X., & Wu, Y. (2013). Bioclogging in porous media under continuous-flow condition. *Environmental Earth Sciences*, *68*(8), 2417–2425. https://doi.org/10.1007/s12665-012-1926-2